Contents lists available at ScienceDirect

Intermetallics

journal homepage: www.elsevier.com/locate/intermet

Positron annihilation study of vacancies in Fe–Al based alloys

O. Melikhova [a], J. Čížek [a,*], J. Kuriplach [a], I. Procházka [a], M. Cieslar [a], W. Anwand [b], G. Brauer [b]

[a] *Charles University in Prague, Faculty of Mathematics and Physics, V Holešovičkách 2, CZ-180 00 Prague 8, Czech Republic*
[b] *Institut für Ionenstrahlphysik und Materialforschung, Forschungszentrum Dresden-Rossendorf, Postfach 510119, D-01314, Dresden, Germany*

ARTICLE INFO

ABSTRACT

In the present contribution, high-resolution positron lifetime and coincidence Doppler broadening spectroscopies are used to characterize defects in $Fe_{76}Al_{24}$ and $Fe_{72}Al_{28}$ alloys. In order to facilitate defect identification, we also perform a theoretical study of basic vacancy-like defects in three phases of the Fe–Al system: ordered, short-range ordered, and disordered. Positron characteristics, like positron lifetime, positron binding energy to defects, high-momentum parts of Doppler broadening curves and specific trapping rates, are calculated for various defect configurations. The results are discussed in the context of experimental data obtained here and available in literature.

© 2009 Elsevier Ltd. All rights reserved.

1. Introduction

Intermetallic alloys based on the Fe–Al system represent perspective materials for industrial applications at elevated temperatures due to a number of advantageous features such as a low density, a high strength and a good corrosion resistance. It is also their low cost, which makes these alloys attractive for industry.

Special importance should be attributed to vacancies in Fe–Al based alloys. The equilibrium concentration of thermal vacancies observed in Fe–Al based alloys at high temperatures appears to be as high as several at% [1], i.e. considerably higher than in pure metals. Such a high concentration of vacancies is a characteristic feature of the Fe–Al based alloys and wields an influence on processes in which diffusion plays a role. Moreover, vacancies and other lattice defects have a significant impact on hardness of Fe–Al based alloys [2]. For example, an extensive attention was paid to the investigation of effect of quenched-in vacancies on hardness of Fe–Al alloys. It turned out that specimens quenched from certain temperature T_Q down to room temperature exhibit a substantial increase in hardness for $T_Q \geq 800\,°C$ [3]. On the other hand, subsequent annealing of quenched specimens at a temperature around 400 °C leads to a decrease in hardness [4]. Some authors argue that such a decrease is due to the formation of a high density of dislocations [5]. Another example of the influence of vacancies on mechanical properties of Fe–Al alloys is an 'anomalous' growth in yield stress at high temperatures. It turns out that such an effect occurs probably due to the formation of a large amount of thermal-equilibrium vacancies [6].

From the above examples it is obvious that a detailed investigation of vacancies and other defects in Fe–Al based alloys is indispensable for a deeper understanding of physical properties of these materials. Positron annihilation spectroscopy (PAS) is a well-recognized, non-destructive method exhibiting very high sensitivity to open-volume defects like vacancies and related defects [7,8]. PAS involves several experimental techniques. Among them, positron lifetime (LT) spectroscopy and coincidence measurements of Doppler broadening of the annihilation radiation (CDB) seem to be the most suitable ones for investigations of vacancies in Fe–Al alloys. The LT spectroscopy makes it possible to identify the type of defects and to determine their concentrations. The LT spectroscopy sensitivity threshold for vacancy concentrations in Fe–Al is about $10^{-6}\,\mathrm{at}^{-1}$. CDB spectroscopy is a unique method which brings information about the local chemical environment of defects. CDB is based on the fact that high momentum parts (HMP) of Doppler broadening profiles, which come from positrons annihilated by core electrons, reflect the electronic structure of a particular element. In other words, it is a kind of 'fingerprint' – a unique characteristic of the particular element. Comparing HMP of these curves with those obtained from standards, i.e. well defined specimens of pure elements, or with those calculated theoretically, the type of atoms in the nearest neighborhood of defects which trap positrons can be determined.

The LT spectroscopy was applied to defect studies in Fe–Al alloys several times [9–12]. For instance, Schaefer et al. [9,10] performed

extensive LT measurements in situ in a wide temperature interval in order to deduce activation energies of vacancy formation and migration in Fe–Al alloys. A LT investigation of binary Fe–Al alloys with varying Al content and quenched from 1000 °C was carried out by Diego et al. [12].

Although previous papers on Fe–Al based alloys have brought a valuable knowledge, one has to state that most of the earlier LT measurements on Fe–Al were performed using spectrometers with relatively pure time resolution (for example 320 ps in [9,10]) and low statistics. Due to these reasons, a reliable decomposition of positron lifetime spectra into individual components could not be performed and only the mean lifetimes (i.e. weighted averages of individual lifetimes) were determined in these works. It was also not possible to include more kinds of defects in the analysis of experimental spectra (e.g. mono- and di-vacancies). Theoretical calculations of positron lifetimes were performed in [12] for several types of defects, for example for different vacancy sites in Al and Fe sublattices as well as for a vacancy-antisite atom defect complex. There are also several CDB studies of defects in Fe–Al systems [13,14]. However, theoretical calculations of HMP curves for various defect configurations in Fe–Al are still missing to our knowledge. Comparison of calculated HMP curves with experimental ones could make it possible to confirm (or to rule out) different hypotheses about what is the dominating type of defects in Fe–Al alloys.

In particular, the aim of the present work is to characterise the nature of defects in quenched-in Fe₃Al based alloys with over- and under-stoichiometric Al content. Defect studies were performed by three complementary PAS techniques: high resolution positron lifetime (LT) spectroscopy, slow positron implantation spectroscopy (SPIS), and coincidence Doppler broadening (CDB). The combination of LT and SPIS enables to determine even a very high concentration of vacancies, while CDB carries information about the local chemical environment of vacancies. PAS investigations were accompanied by Vickers microhardness testing. Lifetime calculations as well as simulations of HMP curves have been performed in order to characterise different vacancy-type defects that can be present in the studied samples.

2. Computational methods

Positron calculations of basic vacancy-like defects in different phases of the Fe₃Al system [15]: ordered (D0₃), short range ordered (B2) and disordered (A2), were performed employing the so-called atomic superposition (ATSUP) method [16]. The lattice parameter used in calculations was $a = 5.792$ Å [17]. We employed the supercell approach, considering 1024 atom-based supercells. Monovacancies were created by removing one Al or Fe atom. Supercells for B2 and A2 structures were prepared by randomly filling atomic positions in the corresponding sublattice.

In the calculations of positron lifetimes and HMP of momentum distribution of annihilating pairs the electron-positron correlations were treated according to Boroński–Nieminen (BN) [18] and according to the gradient-correction (GC) scheme formulated by Barbiellini et al. [19]. The scheme described in [20] was utilized for calculations of HMPs of the momentum distribution of annihilation photons. The calculated spectra were convoluted with a Gaussian function with the width $3.9 \times 10^{-3}\, m_e c$ (full width at half maximum), which corresponds to the experimental energy resolution of our CDB spectrometer. [Ne] orbitals were considered as core states for Al and [Ar] + 3d⁴ ones for Fe.

3. Material and methods

In the present work we studied $Fe_{75.99}Al_{24.01}$ and $Fe_{71.98}Al_{28.02}$ alloys, which represent Fe₃Al based alloys with under-stoichiometric

and over-stoichiometric Al content. Studied alloys were annealed at 1000 °C for 1 h in vacuum (10^{-3} mbar) encapsulated in silicon glass ampoules. The annealing treatment was finished by quenching of the silicon glass ampoule into water of room temperature. As the annealing was performed in the disordered A2 phase region, it is expected that A2 is at least partially retained in the quenched samples. However domains transferred into the B2 phase and even a small fraction of the ordered D0₃ phase should be expected in the quenched samples despite a high cooling rate. Well annealed pure α-Fe (99.99%) and Al (99.9999%) were used as reference specimens in CDB measurements.

A $^{22}Na_2CO_3$ positron source with an activity of 1.2 MBq deposited on a 2 μm thick Mylar foil was used for LT and CDB studies. The source contribution consists of two weak components with lifetimes $\tau_2 \approx 368$ ps and $\tau_3 \approx 1.5$ ns.

A high resolution digital spectrometer [21,22] was employed for LT investigations of studied alloys. The detector part of the digital LT spectrometer is equipped with two Hamamatsu H3378 photo-multipliers coupled with BaF₂ scintillators. Detector pulses are sampled in real time by two ultra-fast 8-bit digitizers Acqiris DC211 with the sampling frequency 4 GHz. The digitized pulses are acquired in a PC and worked out off-line by a software using a new algorithm for integral constant fraction timing [23]. The time resolution of the digital LT spectrometer was 150 ps (FWHM, ²²Na). At least 10^7 annihilation events were accumulated in each LT spectrum.

The CDB spectrometer consists of two HPGe detectors and commercial NIM modules operated by a PC. The overall energy resolution of the spectrometer was 1.0 keV (FWHM) at 511 keV energy. At least 10^8 events were collected in each two-dimensional spectrum, which was subsequently reduced into one-dimensional Doppler profile and instrumental resolution cuts. The relative changes of Doppler profiles were followed as ratio curves of the Doppler profile normalized counts to those of the well annealed α-Fe reference profile. The CDB profiles are symmetrical with respect to the origin and only the parts corresponding to positive Doppler shifts are shown in the paper.

SPIS studies were performed on the magnetically guided variable energy positron beam "SPONSOR" [24]. The energy of incident positrons was varied in the range from 0.03 to 36 keV. The Doppler broadening of the annihilation line was measured by an HPGe detector with an energy resolution of (1.09 ± 0.01) keV at 511 keV and evaluated in terms of the S parameter.

Microhardness was examined using the Vickers method with a loading of 100 g applied for 10 s (HV0.1) using the STRUERS Duramin-2 micro-tester device.

4. Results and discussion

4.1. Theoretical calculations

Fig. 1 shows the unit cell of the D0₃ structure. It consists of two interpenetrating simple cubic sublattices denoted A and B. The Fe and Al occupation of the sites in both sublattices differs in three phases existing in the Fe₃Al system:

In the case of the complete D0₃ order, the A sublattice is occupied exclusively by Fe atoms. The B sublattice consists of alternating sites occupied by Fe and Al atoms. All atoms in the B sublattice are surrounded by 8 nearest neighbor (NN) Fe atoms. Thus one can distinguish two types of Fe atoms in the D0₃ phase: (i) Fe(A) atoms which occupy the A sublattice and are surrounded by 4 NN Fe atoms and 4 NN Al atoms, and (ii) Fe(B) atoms located in the B sublattice surrounded by 8 NN Fe atoms. All Al atoms in the D0₃ phase have 8 NN Fe atoms.
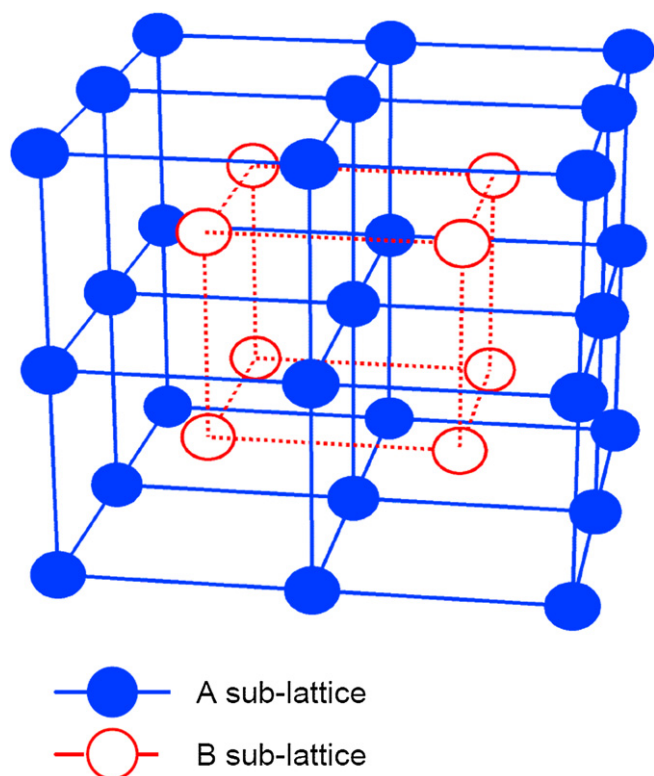
Fig. 1. The unit cell of Fe₃Al based alloys showing A and B sublattices.

As for the B2 order in the Fe₃Al system, Fe and Al atoms occupy all sites in the B sublattice with equal probability, while the A sublattice is occupied only by Fe atoms.

Finally, in the disordered A2 phase all sites in both sublattices are occupied randomly by Fe or Al atoms.

Positron lifetimes were first calculated using both ATSUP–BN and ATSUP–GC approaches. It is known that the GC scheme is more sensitive to details of the electronic structure than local density approximation (LDA) based approaches [25], like the BN one. Therefore, the GC approach should rather be used with self-consistent electron densities. On the other hand, within the BN approach (or an LDA approach in general) one can observe a feed-back effect, which keeps the positron lifetime unchanged independently of small transfers of the electron density [16] (see also [25]). To this end, positron lifetimes calculated by the ATSUP–BN

approach are usually in a better agreement with experiment than lifetimes calculated using the ATSUP–GC approach [25,26]. We can demonstrate this for the case of the bulk lifetime for the D0₃ ordered Fe₃Al alloy. The bulk positron lifetime 110 ps calculated using the ATSUP–BN approach is in good agreement with an experimental value of 112 ps [9], while a bulk lifetime of 118 ps calculated with the ATSUP–GC approach is clearly too long. For these reasons, only lifetimes calculated using the ATSUP–BN approach will be considered in this paper. Bulk positron lifetimes and lifetimes of positrons trapped in vacancies calculated using the ATSUP–BN scheme are collected in Table 1. Positron binding energies to vacancies (E_b) are shown in Table 1 as well. The value of E_b for a given type of vacancy is calculated as a difference of the ground state energy E_0 of the delocalized positron and the energy E_V of the positron trapped in the vacancy considered, i.e.

$$E_b = E_0 - E_V. \tag{1}$$

In the D0₃ phase one can find three types of vacancies: the Al one and two different Fe ones (in A and B sublattice). Lifetimes of positrons trapped in all types of vacancies fall in the relatively narrow range from 182 to 187 ps. The longest positron lifetime was found for the Fe vacancy in the A sublattice, i.e. the only vacancy with some NN Al atoms (all the other types of vacancies have only Fe nearest neighbors). Diego et al. [12] suggested that triple defects consisting of two adjacent Fe vacancies in the A sublattice bound to a NN Al atom in the B sublattice are formed in B2 regions at high temperatures. This defect which corresponds to a Fe divacancy in the D0₃ phase aligned along the [100] direction was also considered in the calculations, see Table 1.

The bulk positron lifetime in the partially ordered B2 phase varies due to the random occupation of the B sublattice sites by Fe and Al atoms. To estimate these variations, we calculated bulk positron lifetimes for a set of randomly generated B2 supercells. The mean value of calculated bulk lifetimes from this set is shown in Table 1 and is very close to the bulk lifetime obtained for the D0₃ phase. The dispersion (standard deviation) of the bulk lifetime in B2 phase was found to be only 0.2 ps. Hence, the effect of the random occupation of the B sublattice sites on the positron lifetime can be considered as negligible.

In the B2 phase one can distinguish Fe vacancies in the A sublattice and vacancies in the B sublattice. The latter vacancies have always 8 NN Fe atoms. On the other hand, number of NN Al and Fe atoms surrounding Fe vacancies in the A sublattice varies randomly. Two extreme cases may be considered for Fe vacancies in the A sublattice in the B2 phase: (i) a vacancy with 8 NN Fe atoms and (ii)

Table 1

Bulk lifetimes, lifetimes of positrons trapped in vacancies, and corresponding positron binding energies (E_b) for vacancies calculated using the ATSUP–BN approach for various phases in Fe₃Al. First and second nearest neighbours of examined vacancy configurations are listed in the second and third column, respectively.

Annihilation site	Vacancy nearest neighbors (NN)	Vacancy next nearest neighbors (2 NN)	τ (ps)	E_b (eV)
D0₃ phase				
Bulk			110	–
Fe vacancy (A sublattice)	4 Al + 4 Fe	8 Fe	187	3.1
Fe vacancy (B sublattice)	8 Fe	8 Al	185	3.2
Al vacancy (B sublattice)	8 Fe	8 Fe	182	3.5
Fe divacancy (A sublattice) in [100] direction	6 Fe + 6 Al	10 Fe	195	4.0
B2 phase				
Bulk			109	–
Fe vacancy (A sublattice)	8 Fe	8 Fe	181	3.1
Fe vacancy (A sublattice)	8 Al	8 Fe	193	2.7
vacancy in B sublattice	8 Fe	8 Fe	182	3.5
vacancy in B sublattice	8 Fe	8 Al	185	3.1
A2 phase				
Bulk			108	–
Vacancy	8 Fe	8 Fe	181	3.1
Vacancy	8 Al	8 Al	199	3.6
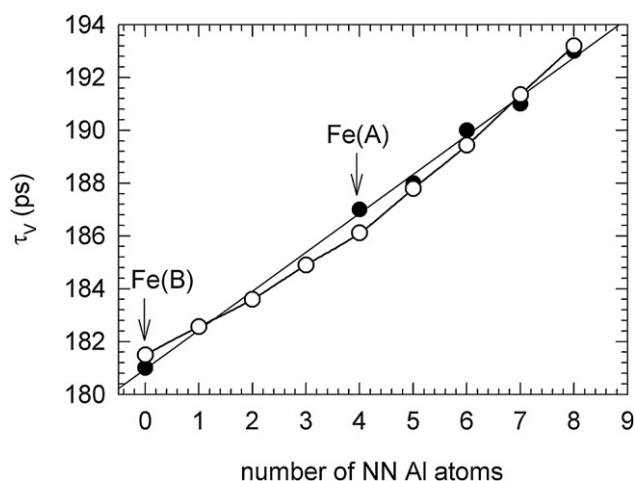
Fig. 2. Calculated lifetimes of positrons trapped in Fe vacancies as a function of the number of NN Al atoms around vacancies. Open circles – B2 phase, Full circles D0$_3$ phase: Fe(A), Fe(B) vacancy and Fe(A) vacancy with various number of Al antisites.

Fig. 3. Calculated HMP ratio curves (related to pure Fe) for various positron states in the D0$_3$ phase. The HMP curve for pure Al is plotted as well for comparison.

a vacancy with 8 NN Al atoms. The local surrounding of Fe vacancies in the A sublattice varies between these two extremes, thereby, the lifetime of trapped positrons is expected to vary between the lifetimes of positrons trapped in Fe vacancy (i) and (ii), i.e. in the range from 181 to 193 ps (see Table 1). Fig. 2 shows lifetimes of positrons trapped in the Fe vacancy as a function of the number of NN Al atoms surrounding the vacancy. It is clear that the positron lifetime increases with the increasing number of NN Al atoms. It should be noted that while 2 NN of Fe vacancies considered in Fig. 2 are always Fe atoms (sites on the A sublattice), occupation of third and higher-order NN vary due to the random occupation of the B sublattice sites. Nevertheless, we found that the dispersion of positron lifetimes due to this effect is lower than 0.1 ps for all vacancies considered in Fig. 2. Thus, the lifetime of trapped positrons is determined predominantly by NN and 2 NN atoms surrounding vacancy. Fe vacancies in the A sublattice in the D0$_3$ phase are always surrounded by 4 NN Al atoms. Hence, the Fe- vacancy in the A sublattice surrounded by more than 4 NN Al atoms may be considered also as a vacancy in the D0$_3$ phase with corresponding number of Al antisite atoms. For example, an Fe vacancy in the A sublattice surrounded by 6 NN Al atoms can be considered also as an Fe(A) vacancy in the D0$_3$ phase with two Al antisite atoms. Lifetimes of positrons trapped in Fe vacancies in the D0$_3$ phase with various number of Al antisite atoms are shown in Fig. 2 as well. Clearly, these lifetimes differ only very slightly from those calculated for Fe vacancies in B2 phase surrounded by the same number of NN Al atoms.

The bulk positron lifetime in the disordered A2 phase fluctuates due to the random distribution of Fe and Al atoms. However, similarly to the B2 phase these fluctuations are rather small. The dispersion (standard deviation) of bulk positron lifetimes obtained from a set of randomly generated A2 supercells is only 0.3 ps. The mean value of bulk positron lifetimes for the A2 phase is shown in Table 1.

Two extreme cases can be considered for vacancies in the A2 phase: (i) a vacancy completely surrounded by Fe atoms (i.e. 8 NN Fe + 8 2 NN Fe atoms), and (ii) a vacancy completely surrounded by Al atoms (i.e. 8 NN Al + 8 2 NN Al atoms). Positron lifetimes for these two extremes are shown in Table 1. The lifetime of positrons trapped in a vacancy in the A2 phase varies between these extremes, i.e. in the range from 181 to 199 ps.

Calculated HMP ratio curves (related to pure Fe) for the D0$_3$ phase are plotted in Fig. 3. The HMP curve calculated for pure Al is plotted in Fig. 3 as well. It should be mentioned that calculated HMP
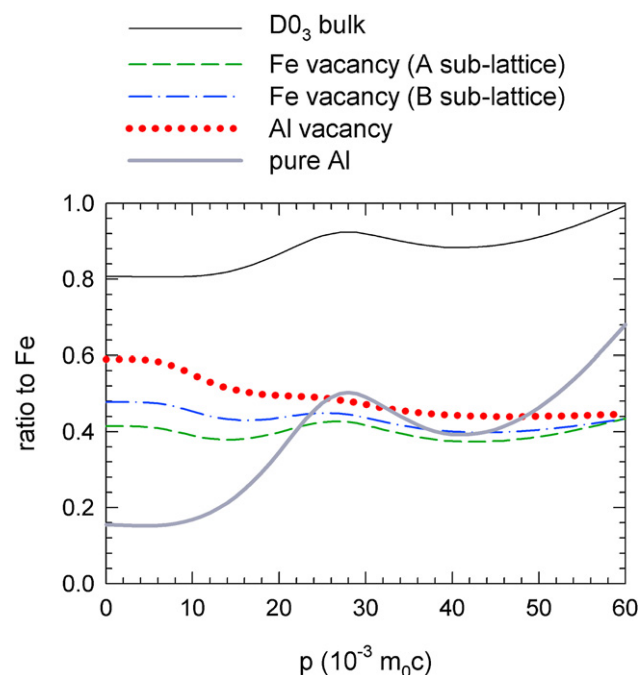
curves represent only the contribution of core electrons. Therefore, a comparison with experiment is meaningful only in the high momentum range $p \geq 20 \times 10^{-3} \, m_0 c$ where the contribution of core electrons dominates. The main feature of the contribution of positrons annihilated by Al electrons is a local maximum at $p \approx 28 \times 10^{-3} \, m_0 c$. This local maximum is absent in the Al vacancy because it is completely surrounded by Fe (all NN and 2 NN sites are occupied by Fe, see Table 1 and Fig. 1). On the other hand, HMP curves for both kinds of Fe vacancies exhibit such a local maximum at $p \approx 28 \times 10^{-3} \, m_0 c$, but it is more pronounced in the Fe vacancy in the A sublattice because it has 4 NN Al atoms, while the Fe vacancy in the B sublattice has Al atoms only in 2 NN positions. Hence, the local maximum at $p \approx 28 \times 10^{-3} \, m_0 c$ is a sign which testifies the presence of Al atoms in the vicinity of the vacancy.

The calculated HMP ratio curves for the Fe vacancy in the A sublattice are plotted in Fig. 4 as a function of the number of NN Al atoms surrounding the vacancy. Clearly, the peak at $p \approx 28 \times 10^{-3} \, m_0 c$ becomes more pronounced with the increasing number of NN Al atoms. Simultaneously the HMP ratio curves are shifted down with the increasing number of NN Al atoms. This is due to a less number of Al core electrons compared to Fe.

4.2. LT and SPIS results

Both quenched alloys exhibit a single component LT spectrum with the corresponding positron lifetime τ_V shown in Table 2. The lifetimes τ_V in both alloys are significantly longer than the Fe$_3$Al bulk positron lifetime $\tau_B = 112$ ps [9] and fall into the range expected for vacancies. Hence, both alloys contain a high density of quenched-in vacancies, which causes saturated positron trapping. Comparison with theoretical calculations shows that experimental lifetimes τ_V are compatible with Fe vacancy in the B2 phase surrounded by 7 or 8 NN Al atoms, see Table 1. Another possibility is that positrons are trapped in [001] Fe divacancies in the ordered D0$_3$ phase.

The dependence of the S parameter on the energy of incident positrons measured by SPIS on quenched Fe$_{75.99}$Al$_{24.01}$ and Fe$_{71.98}$Al$_{28.02}$ alloys is plotted in Fig. 5. A local minimum of S at low
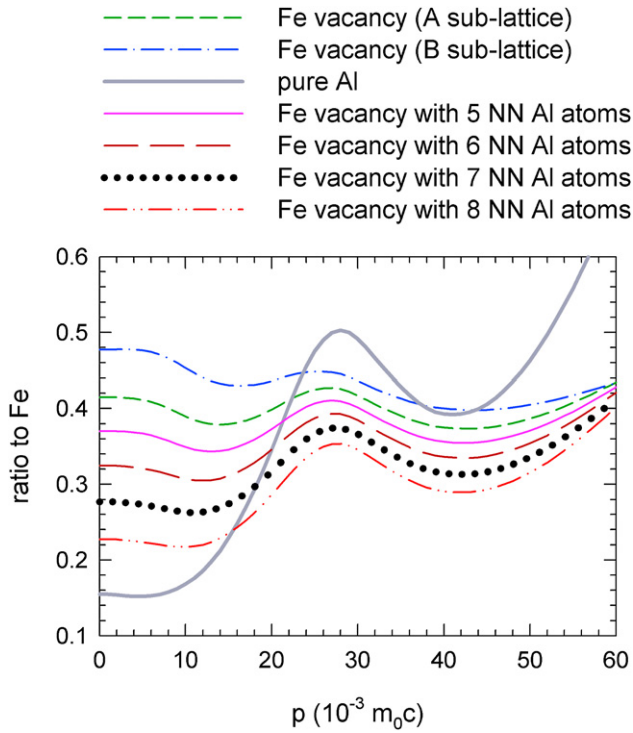
Fig. 4. Calculated HMP ratio curves (related to pure Fe) for the Fe vacancy in the A sublattice as a function of the number of NN Al atoms surrounding the vacancy. The HMP curve for pure Al is plotted as well for comparison.

energies 1–2 keV is due to positron annihilations in a thin oxide layer formed on the surface during annealing. One can see in Fig. 6 that the bulk value of the S parameter is higher in the $Fe_{71.98}Al_{28.02}$ alloy, i.e. in the alloy with higher Al content. The $S(E)$ curves were fitted by the VEPFIT software package [27] assuming two layers: (i) a thin oxide layer on surface, and (ii) the bulk alloy. In both alloys we obtained a good fit, which is plotted by solid lines in Fig. 5. Thickness of the oxide layer is around 10 nm and 30 nm in the $Fe_{71.98}Al_{28.02}$ and $Fe_{75.99}Al_{24.01}$ alloy, respectively. The positron diffusion lengths obtained from fits of the S(E) curves in both alloys are shown in Table 2. The $Fe_{71.98}Al_{28.02}$ alloy exhibits a shorter diffusion length than the $Fe_{75.99}Al_{24.01}$ alloy. This indicates that the $Fe_{71.98}Al_{28.02}$ alloy, i.e. the alloy with an enhanced Al content, contains more quenched-in vacancies compared to the other alloy.

4.3. Estimation of concentration of quenched-in vacancies

The limit of vacancy concentration which causes saturated positron trapping can be estimated from the two-state trapping model. The positron trapping rate to vacancies can be calculated from the following equation

$$K = \frac{I_2}{I_1}\left(\frac{1}{\tau_B} - \frac{1}{\tau_V}\right) \tag{2}$$

Table 2
Summarized experimental results for quenched $Fe_{75.99}Al_{24.01}$ and $Fe_{71.98}Al_{28.02}$ alloys: experimental lifetimes of positrons trapped at vacancies (τ_V), fraction of positrons annihilating with Al electrons obtained from fitting of CDB spectra using Eq. (8) (ξ_{Al}), positron diffusion length measured by SPIS (L_+), concentration of vacancies (c_V) calculated from SPIS data, and microhardness (HV0.1).

Sample	τ_V (ps)	ξ_{Al}	L_+ (nm)	c_V (at.$^{-1}$)	HV0.1
$Fe_{75.99}Al_{24.01}$	190.8 ± 0.4	0.89 ± 0.01	40 ± 6	$(4.8 \pm 0.6) \times 10^{-4}$	412 ± 5
$Fe_{71.98}Al_{28.02}$	195.3 ± 0.5	0.95 ± 0.01	4.0 ± 0.2	$(5.0 \pm 0.5) \times 10^{-2}$	491 ± 5
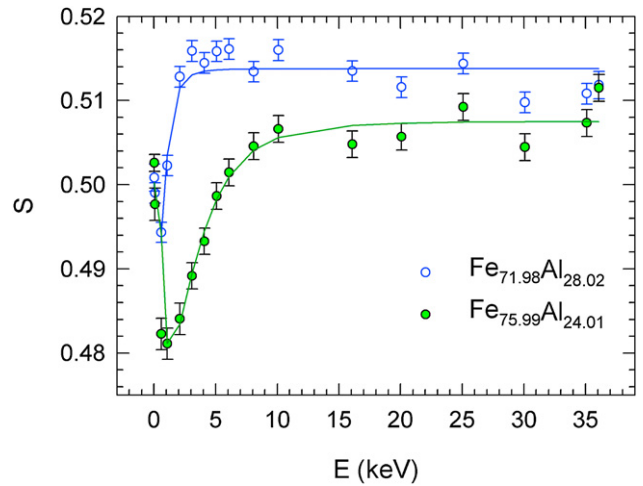
Fig. 5. The dependence of the S parameter on the incident positron energy for $Fe_{75.99}Al_{24.01}$ and $Fe_{71.98}Al_{28.02}$ alloys measured by SPIS.

where $\tau_B = 112$ ps is the positron bulk lifetime in Fe_3Al [9]. The free positron component cannot be resolved in an LT spectrum if its relative intensity I_1 falls below $\approx 5\%$. This corresponds to the positron trapping rate $K_{max,LT} \approx 7 \times 10^{10}$ at s^{-1}. If the trapping rate $K \geq K_{max,LT}$, then saturated positron trapping in vacancies takes place. The lowest concentration of vacancies which causes saturated positron trapping is

$$c_{Vmax,LT} = \frac{K_{max,LT}}{\nu_V} \approx 2 \times 10^{-4} at.^{-1} \tag{3}$$

where we used the specific positron trapping rate $\nu_V = 4 \times 10^{14}$ at s^{-1}, reported for vacancies in Fe_3Al in Ref. [9]. Clearly, the concentration of quenched-in vacancies in both alloys is higher than $c_{Vmax,LT}$.

The positron trapping rate K to vacancies can be also calculated from SPIS results
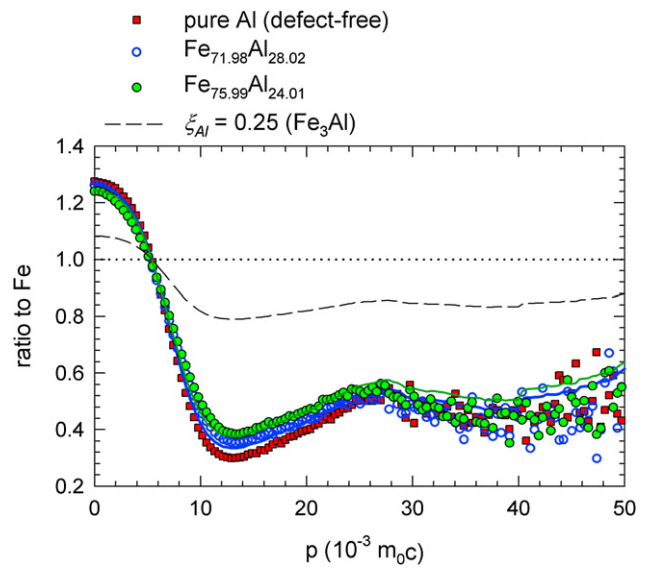
Fig. 6. CDB ratio curves (related to well annealed pure Fe) for $Fe_{75.99}Al_{24.01}$ and $Fe_{71.98}Al_{28.02}$ alloys. The ratio curve for well annealed pure Al is plotted as well. The curve corresponding to the fraction of positrons annihilated by Al electrons $\xi_{Al} = 0.25$ corresponding to the Al atomic concentration in Fe_3Al is plotted for comparison. The solid lines represent the best approximation of the experimental curves by Eq. (8).

$$K = \frac{1}{\tau_B}\left(\frac{L_{+,B}^2}{L_+^2} - 1\right) \tag{4}$$

Here $L_{+,B}$ is the positron diffusion length in the defect-free material and L_+ is the positron diffusion length measured in the studied sample. The diffusion length $L_{+,B}$ is given by the equation

$$L_{+,B} = \sqrt{D_+ \tau_B} \tag{5}$$

The positron diffusion coefficient D_+ in Fe$_3$Al was estimated as a weighted average of positron diffusion coefficients in Fe and Al

$$D_+ \approx \frac{3}{4}D_{+,Fe} + \frac{1}{4}D_{+,Al} = 3 \text{cm}^2 \text{ s}^{-1} \tag{6}$$

The positron diffusion coefficients for pure Fe and Al were calculated using the deformation potential approximation [28].

The shortest positron diffusion length which can be determined by SPIS is $L_+ \approx 1$ nm. This corresponds to a limiting positron trapping rate $K_{max,SPIS} \approx 3 \times 10^{14}$ at s^{-1}. Hence, using SPIS it is possible to determine even very high concentrations of vacancies. The upper limit of vacancy concentration measurable by SPIS is

$$c_{Vmax,SPIS} = \frac{K_{max,SPIS}}{\nu_V} \approx 0.7 \text{at.}^{-1}. \tag{7}$$

Obviously the upper limit given by Eq. (7) is extremely high concentration, which cannot be reached in any real material. Thus, we can conclude that SPIS is able to determine even very high concentrations of vacancies and there is actually no upper limit of vacancy concentration measurable by this technique.

The concentration of quenched-in vacancies in the studied alloys determined from SPIS results is shown in Table 2. Both studied alloys exhibit significant concentrations of vacancies, in particular Fe$_{71.98}$Al$_{28.02}$ contains extremely high concentration of vacancies, which is two orders of magnitude higher than in Fe$_{75.99}$Al$_{24.01}$. A higher concentration of vacancies in Fe$_{71.98}$Al$_{28.02}$ alloy is in concordance with higher hardness measured on this alloy. Hence, the concentration of vacancies and the hardness of the alloy increase with the increasing Al content.

4.4. CDB results

Fig. 6 shows CDB ratio curves (with respect to the reference pure Fe sample) measured on Fe$_{75.99}$Al$_{24.01}$ and Fe$_{71.98}$Al$_{28.02}$ alloys. The CDB curve for pure Al is shown in Fig. 6 as well. The shape of CDB curves for both alloys is very close to that for pure Al. It gives clear evidence that positrons annihilate predominantly with Al electrons. Hence, quenched-in vacancies in both alloys are surrounded mostly by Al atoms. The dashed line in Fig. 6 shows for comparison a hypothetical Fe$_3$Al profile created using Fe and Al ones considering the 25% fraction of positron annihilation with Al electrons, i.e. in the case of no enhancement of Al atoms around vacancies.

In the first approximation the CDB ratio curve ρ for the studied alloys can be expressed as

$$\rho \approx \zeta_{Al}\rho_{Al} + 1 - \zeta_{Al}, \tag{8}$$

where ρ_{Al} is the ratio curve for pure Al and ξ_{Al} is the fraction of positrons annihilating with Al electrons. Solid lines in Fig. 6 show the best approximation of experimental curves by Eq. (8). It is clear that the approximation by Eq. (8) is very good in the high momentum region ($p > 15 \times 10^{-3}$ m_0c), but some differences can bee seen in the low momentum region. Such deviations are due to the fact that the ρ_{Al} curve was measured on defect-free pure Al, while in the studied alloys positrons are trapped in vacancies. The fractions ξ_{Al} obtained from fits of CDB ratio curves of both alloys are
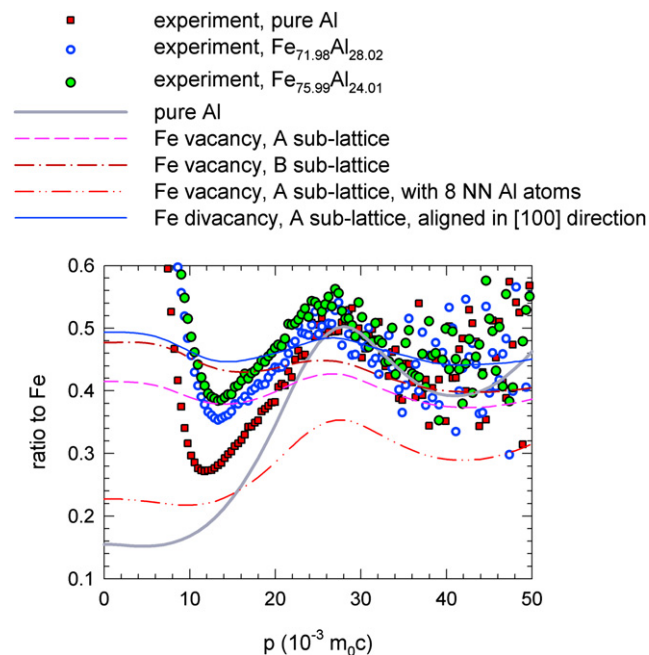
Fig. 7. Comparison of experimental CDB ratio curves (related to well annealed pure Fe) with calculated HMP curves. Lines show calculated HMP curves, while scattered plots are experimental results.

listed in Table 2. High fractions ξ_{Al} in both alloys testify that quenched-in vacancies are almost completely surrounded Al atoms. A slightly higher ξ_{Al} value obtained in Fe$_{71.98}$Al$_{28.02}$ is in concordance with a higher Al content in this alloy. Hence, CDB results proved that vacancies in A2 and B2 phase are preferentially surrounded by Al atoms. This is consistent with lifetimes in the range 191–195 ps measured by LT spectroscopy, which corresponds to the calculated lifetime for the Fe vacancy surrounded by 7–8 NN Al atoms (see Fig. 2). Hence, there is an attractive interaction between vacancies and Al atoms. It should be mentioned that positron lifetimes measured in the quenched alloys are close also to the calculated lifetime for Fe divacancies in the A sublattice in D0$_3$ phase aligned in [100] direction, see Table 1. However, these defects have 6 NN Al atoms and 6 NN Fe atoms. Consequently, a significant fraction of positrons trapped in Fe divacancies annihilate with Fe atoms, which is in contradiction with the experimental CDB curves. Thus, Fe divacancies are ruled out as possible candidates for defects in the quenched alloys.

A comparison of experimental CDB curves with calculated HMP curves for selected defects is presented in Fig. 7. Obviously there is a good agreement of the calculated HMP curve for pure Al with the corresponding experimental CDB curve in the high momentum range $p \geq 20 \times 10^{-3}$ m_0c, where the contribution of annihilations with core electrons dominates. Agreement of calculated HMP for pure Fe with experiment is slightly worse, because ATSUP approach is unable to describe accurately the semi-core 3d electrons. Furthermore, calculated HMP curves for various kinds of vacancies are compared with experimental curves in Fig. 7. Obviously, calculated HMP curves exhibit a local maximum at $p \approx 28 \times 10^{-3}$ m_0c in good agreement with experiment. As shown in Section 4.1, a peak at this momentum is a sign of Al atoms surrounding the vacancy. However, it is clear from Fig. 7 that the contribution of Al electrons is systematically underestimated in calculated profiles. This can be attributed to two effects which were neglected in the present ATSUP approach: (i) a charge transfer among Al and Fe atoms, and (ii) ion relaxations around vacancies. Both these effects seem to play an

important role in Fe$_3$Al based alloys and should be included in future refined calculations. Because of the reasons explained above, a comparison of the HMP curves calculated by the ATSUP approach with experiment can be done on a qualitative base only. One can see in Fig. 7 that the Fe vacancy in the A sublattice surrounded by 8 NN Al atoms exhibits the most pronounced peak at $p \approx 28 \times 10^{-3}\ m_0 c$, which is related to Al electrons. This peak is too small for all the other HMP curves shown in Fig. 7, because all these other defects (including the [100] Fe divacancy in the A sublattice) are characterized by a significant contribution of annihilations with Fe electrons. However, no significant contribution of Fe electrons was observed in experiment. Hence, qualitative analysis of HMP curves indicates that quenched-in defects in the studied alloys are Fe vacancies in the A sublattice surrounded by NN Al atoms.

Note that first principles theoretical calculations performed by several authors [29–31] shown that the formation energy of Al vacancies is significantly higher than the formation energy of Fe vacancies. Thus, it is expected that Fe$_3$Al based alloys contain predominantly Fe vacancies. Our results are in agreement with this theoretical prediction: We do not observe Al vacancies despite the fact that they are deeper positron traps than Fe vacancies.

5. Conclusions

In the present work we studied Fe$_{75.99}$Al$_{24.01}$ and Fe$_{71.98}$Al$_{28.02}$ alloys quenched from 1000 °C. Both alloys contain a high concentration of quenched-in Fe vacancies, which are surrounded by the nearest neighbor Al atoms. The concentration of quenched-in vacancies was determined from positron diffusion length measured by SPIS. The Fe$_{71.98}$Al$_{28.02}$ alloy exhibits significantly higher concentration of vacancies. Thus, the vacancy concentration increases with the increasing Al content. A higher concentration of vacancies in Fe$_{71.98}$Al$_{28.02}$ alloy is in concordance with higher hardness measured on this alloy. This testifies a strong influence of vacancies on mechanical properties of Fe$_3$Al based alloys.

Acknowledgement

References

[1] Ho K, Dodd RA. Scr Metall 1978;12:1055.
[2] Liu T, Lee EH, McKammy CG. Scr Metall 1989;23:875.
[3] Jordan JL, Derbi SC. Intermetallics 2003;11:507.
[4] Sassi O, Aride J, Bernardini J, Moya G. Ann Chim Sci Mat 1998;23:421.
[5] Morris MA, Morris DG. Scr Metall 1998;38:509.
[6] Yoshimi K, Hanada S, Yoo MH. Intermetallics 1996;4:159.
[7] Hautojärvi P. In: Hautojärvi P, editor. Positrons in solids. Berlin: Springer-Verlag; 1979.
[8] Hautojärvi P, Corbel C. In: Dupasquier A, Mills AP, editors. Positron spectroscopy of solids, proceedings of the international school of physics "enrico fermi". Amsterdam: IOS Press; 1995. p. p 491.
[9] Schaefer HE, Würschum R, Šob M, Žák T, Yu WZ, Eckert W, et al. Phys Rev B: Condens Mater 1990;41:11869.
[10] Schaefer HE, Damson B, Weller M, Arzt E, George EP. Phys Status Solidi 1997;160:531.
[11] Jirásková Y, Schneeweiss O, Šob M, Novotný I, Procházka I, Bečvář F, et al. J Phys 1995;5:C1–157.
[12] de Diego N, Plazaola F, Jiménez JA, Serna J, del Río J. Acta Mater 2005;53:163.
[13] Gialanella S, Brusa RS, Deng W, Marino F, Spataru T, Principi G. J Alloys Compds 2001;317–318:485.
[14] Somieski B, Schneibel JH, Hulett LD. Phil Mag Lett 1999;79:115;
Massalski TB, editor. Binary alloy phase diagrams. Metals Park, Ohio: Americal Society for Metals; 1986.
[15] Puska MJ, Nieminen RM. J Phys F 1983;13:333.
[16] Seitsonen AP, Puska MJ, Nieminen RM. Phys Rev B: Condens Mater 1995;51:14057.
[17] Wakiyama T. J Phys Soc Jpn 1972;32:1222.
[18] Boroński E, Nieminen RM. Phys Rev B: Condens Mater 1986;34:3820.
[19] Barbiellini B, Puska MJ, Torsti T, Nieminen RM. Phys Rev B: Condens Mater 1995;51:7341.
[20] Kuriplach J, Morales AL, Dauwe C, Segers D, Šob M. Phys Rev B: Condens Mater 1998;58:107475.
[21] Bečvář F, Čížek J, Procházka I, Janotová J. Nucl Instrum Methods A 2005;539:372.
[22] Bečvář F, Čížek J, Procházka I. Acta Phys Pol A 2008;113:1279.
[23] Bečvář F. Nucl Instrum Methods B 2007;261:871.
[24] Anwand W, Kissener HR, Brauer G. Acta Physica Polonica A 1995;88:7.
[25] Barbiellini B, Puska MJ, Korhonen T, Harju A, Torsti T, Nieminen RM. Phys Rev B: Condens Mater 1996;53:16201.
[26] Campillo Robles JM, Odo E, Plazaola F. J Phys Condens Matter 2007;19: 176222.
[27] van Veen A, Schut H, Clement M, de Nijs J, Kruseman A, Ijpma M. Appl Surf Sci 1995;85:216.
[28] Bardeen J, Shockley W. Phys Rev 1950;80:72.
[29] Mayer J, Elsässer C, Fähnle M. Phys Status Solidi 1995;191:283.
[30] Krachler R, Ipser H. Intermetallics 1999;7:141.
[31] Fähnle M, Mayer J, Meyer B. Intermetallics 1999;7:315.